WILEY

RESEARCH ARTICLE OPEN ACCESS

Development of Broad-Spectrum β-Cyclodextrins-Based Nanomaterials Against Influenza Viruses

Arnaud Charles-Antoine Zwygart[1] (iD) | Chiara Medaglia[1] | Yong Zhu[2] | E. Bart Tarbet[3] | Westover Jonna[3] | Clément Fage[1] | Didier Le Roy[4] | Thierry Roger[4] | Sophie Clément[1] | Samuel Constant[5] | Song Huang[5] | Francesco Stellacci[2] | Paulo Jacob Silva[2] | Caroline Tapparel[1]

[1]Department of Microbiology and Molecular Medicine, University of Geneva, Geneva, Switzerland | [2]Institute of Materials, Ecole polytechnique fédérale de Lausanne, Lausanne, Switzerland | [3]Department of Animal, Dairy, and Veterinary Sciences, Institute for Antiviral Research, Utah State University, Logan, Utah, USA | [4]Infectious Diseases Service, Department of Medicine, Lausanne University Hospital and University of Lausanne, Lausanne, Switzerland | [5]Epithelix Sas, Geneva, Switzerland

Correspondence: Caroline Tapparel (caroline.tapparel@unige.ch)

ABSTRACT

In recent decades, epidemics and pandemics have multiplied throughout the world, with viruses generally being the primary responsible agents. Among these, influenza viruses play a key role, as they potentially cause severe respiratory distress, representing a major threat to public health. Our study aims to develop new broad-spectrum antivirals against influenza to improve the response to viral disease outbreaks. We engineered macromolecules (named CD-SA) consisting of a β-cyclodextrin scaffold modified with hydrophobic linkers in the primary face, onto which unitary sialic acid epitopes are covalently grafted to mimic influenza virus−host receptors. We assessed the antiviral efficacy, mechanism of action, and the genetic barrier to resistance of this compound against influenza in vitro, ex vivo, and in vivo. We demonstrated that CD-SA, with a unitary SA, without extensive polysaccharides or specific connectivity, acts as a potent virucidal antiviral against several human influenza A and B viruses. Additionally, CD-SA displayed antiviral activity against SARS-CoV-2, a virus that also relies on sialic acid for attachment. We then assessed the genetic barrier to resistance for CD-SA. While resistance emerged after six passages with CD-SA alone, the virus remained sensitive through eight passages when co-treated with interferon-λ1 (IFN λ1). Finally, we completed the characterization of the antiviral activity by conducting both ex vivo and in vivo studies, demonstrating a potent antiviral effect in human airway epithelia and in a mouse model of infection, higher than that of Oseltamivir, a currently approved anti-influenza antiviral. The findings presented in this study support the potential therapeutic utility of a novel β-cyclodextrin-based nanomaterial for the treatment of influenza infections and potentially other sialic acid-dependent viruses.

1 | Introduction

Over the last decades, epidemics and pandemics caused by viral pathogens have risen drastically. Globalization increases the circulation of people and goods which offers infectious agents a constant avenue to spread worldwide [1]. It is difficult to predict which virus will trigger the next pandemic, but influenza viruses (IVs) are among the most likely candidates. IVs cause annual epidemics during the cold season and have been responsible for four pandemics in the last century [2, 3]. IV targets respiratory epithelial cells. The infection can cause mild illness in the upper airways but can lead to severe complications like pneumonia and respiratory failure if it reaches the lungs [4]. Additionally, the virus kills ciliated cells weakening the respiratory barrier and making the host more susceptible to secondary infections by other pathogens, which worsen the outcome [5, 6]. Given this scenario, ready-to-use antivirals active against several IV types/subtypes are needed to relieve the human and economic burden caused by this disease.

IV is a negative single-stranded RNA virus with an external envelope decorated with the hemagglutinin (HA) and neuraminidase (NA) proteins, which mediate viral attachment and release, respectively. HA recognizes terminal sialic acids (SA) attached to galactose residue [7, 8]. Human IVs bind to α2-6 linked SA, while avian IVs interact with α2-3 linked SA. These linked SA are heterogeneously distributed in the human respiratory tract. α2-6 linkages decrease from upper to lower respiratory system, reaching an approximately equal ratio to of α2-3 linkages in the alveoli [8, 9].

In previous studies, we reported CD-6′SLN [10–12], an antiviral molecule that mimics the attachment moieties of HA from human IV. This compound is made of a β-cyclodextrin core (CD) grafted with long alkyl chains terminating in 6′SLN (6'-Sialyl-N-acetyllactosamine, a trisaccharide terminating with an α2-6 SA) (Figure 1B). This approach allowed trapping and irreversibly damaging viruses, thereby preventing them from attaching to host cells. This resulted in potent antiviral activity

in cell lines, in ex vivo reconstituted human respiratory epithelia and in mice [10, 11, 13].

In the current study, we investigated the efficacy and the mechanism of action of CD-SA, a novel CD-based molecule grafted with long alkyl chains terminating in a single residue of SA (Figure 1A). The molecular arrangement of CD-SA should allow binding to the HA pocket of a broad range of IV strains and even to other SA-dependent viruses such as SARS-CoV-2 [14] or Human Parainfluenza Virus type 3 (HPIV3) [15, 16]. Additionally, it may present a higher barrier to antiviral resistance by preventing the receptor switch from α2-6 to α2-3 SA. We confirmed the antiviral activity of CD-SA ex vivo and in vivo and demonstrated that its genetic barrier to antiviral resistance is higher than that of CD-6′SLN.

2 | Materials and Methods

The synthesis of CD-SA as well as more detailed methodologies are available in the Supporting Information File.

2.1 | Cells and Tissues

Culture conditions of Madin-Darby canine kidney (MDCK, ATCC), A549 cells (ATCC), Vero E6 expressing TMPRSS2, kindly provided by Prof. Isabella Eckerle (University of Geneva, Switzerland) and Calu-3 cells (ATCC) are described in the Supporting Information File.

Human airway epithelia (HAE) (MucilAir, Epithelix, Plan-les-Ouates, Switzerland) were reconstituted from freshly isolated primary human nasal polyp epithelium collected either from 14 different donors upon surgical nasal polypectomy or from individual donors. The donor patients presented no atopy, asthma, allergy, or other known comorbidities. The study was conducted according to the Declaration of Helsinki on
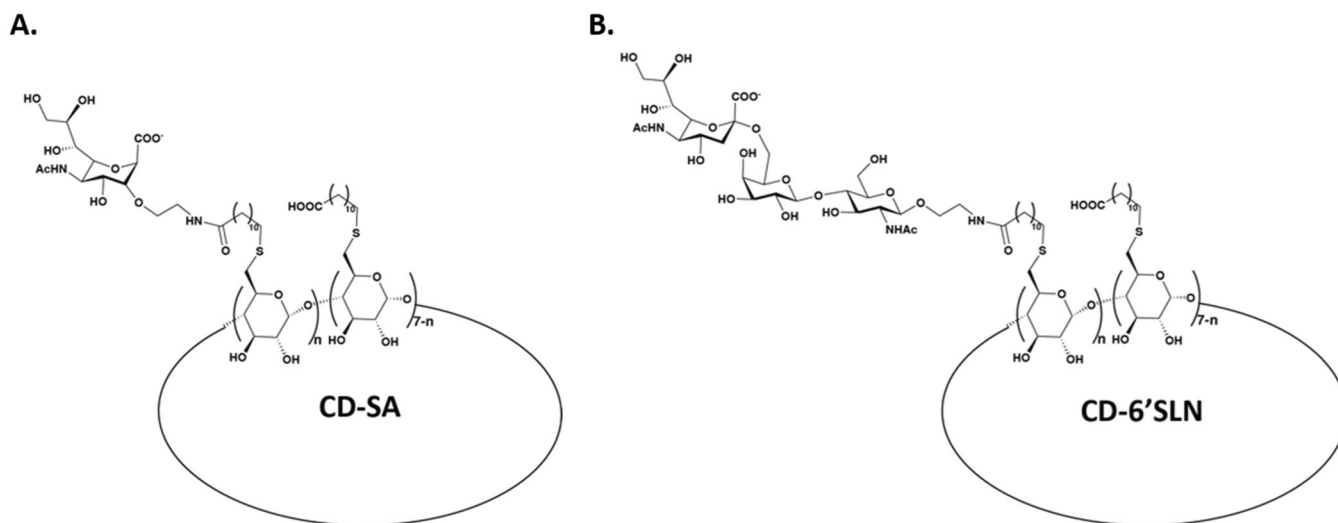

FIGURE 1 | Schematic representation of CD-SA and CD-6′SLN. A β-CD core is modified on its primary face with hydrophobic undecyl linkers exposing either a single sialic acid residue for CD-SA (A) or 6′SLN (6'-Sialyl-N-acetyllactosamine), a trisaccharide terminating with an α2-6 sialic acid for CD-6′SLN (B) [10].

biomedical research (Hong Kong amendment, 1989), and the research protocol was approved by the local ethics committee. The tissues were maintained at the air-liquid interface according to the manufacturer's instructions [5].

2.2 | Viruses

Human A/Netherlands/602/2009 (H1N1) pdm09 influenza virus (N09), human A/Wyoming/03/2003 (H3N2) and human B/Wisconsin/01/2010 B/Yamagata-lineage were provided by Prof. Mirco Schmolke (University of Geneva, Switzerland). Human A/Switzerland/02824/2022 (H1N1)pdm09, human A/Switzerland/4955/2019 (H3N2), human B/Switzerland/88277/2018 Yamagata-lineage, human B/Switzerland/47324/2024 Victoria-Lineage and HPIV3 were provided by the University Hospital of Geneva. hCoV-19/Switzerland/VD-HUG-36221084/2021 (Omicron B.A.1 Variant) was kindly provided by Prof. Isabella Eckerle (University of Geneva, Switzerland).

For in vivo experiments, mouse adapted influenza A/California/04/2009 (H1N1)pdm09 was provided by Dr. Elena Govorkova (St. Jude Children's Research Hospital, Memphis, TN).

Detailed procedure of viral stock production is available in the Supporting Information File.

2.3 | Cell Viability Assay

Viability in cells and ex vivo tissues were assessed by Resazurin assay as described [17]. Detailed procedure is available in the Supporting Information File.

2.4 | Antiviral Dose Response Assays

The viral inhibition assays for A/Netherlands/602/2009 (H1N1) pdm09, A/Switzerland/02824/2022 (H1N1)pdm09, A/Switzerland/4955/2019 (H3N2) and B/Wisconsin/01/2010 Yamagata-lineage were performed as described [10]. The viral inhibition assays for A/Wyoming/03/2003 (H3N2), B/Switzerland/88277/2018 Yamagata-lineage and B/Switzerland/47324/2024 Victoria-Lineage were performed the same way, except that the analysis was obtained by immunofluorescence staining. For Omicron B.A.1 and HPIV3 inhibition assays, the same procedure was applied in Vero E6 cells expressing TMPRSS2 and A549 cells, respectively and analysis was performed by focus-forming unit (FFU) assay. Detailed procedures are available in the Supporting Information File.

2.5 | Ex Vivo Antiviral Testing Assay

MucilAir tissues were infected apically with 1E5 RNA copies/tissue of N09 in MucilAir medium (Epithelix), at 37°C for 5 h. After inoculum removal, the apical side was washed three times with PBS and 1 µg/µL of CD-SA11 or CD-6′SLN were administered apically. Viruses released apically were harvested daily, and tissues were treated with fresh drugs. Viral loads were assessed by RT-qPCR.

2.6 | Virucidal Assay

1E6 PFU of virus was incubated with one EC_{90} of CD-SA or CD-6′SLN for 3 h at 37°C. The mixture was then serially diluted in serum-free DMEM and transferred on MDCK cells, seeded in a 96-multiwell plate. After 1 h, the mixture was removed and fresh medium was added. At 16 hpi, viral titers were evaluated by immunocytochemistry, and percentages of infection were calculated compared to the untreated control (incubated 3 h at 37°C with buffer). For A/Wyoming/03/2003 (H3N2), B/Switzerland/88277/2018 Yamagata-lineage and B/Switzerland/47324/2024 Victoria-Lineage, the same procedure was applied, except that the number of infected cells was obtained by immunofluorescence as in §2.4.

For Omicron B.A.1, the same procedure was applied as in §2.4.

2.7 | RNA Exposure Assay

N09 (1E6 PFU/mL) was incubated with either 100 µg/mL of CD-SA or sodium dodecyl sulfate (SDS, used as positive control) in DMEM medium at 37°C for 3 h. Half of the mixture was treated with 10 mg/mL RNAse A (EN0531, Thermo Fisher Scientific, Waltham, MA) and the other half with buffer. After 30 min at 37°C, 500 µL of GTC lysis buffer (Omega bio-tek, Norcross, GA) was added, and RNA was extracted and quantified by RT-qPCR.

2.8 | Transmission Electron Microscopy (TEM) Assay

TEM was performed at the Dubochet Center for Imaging (DCI Geneva) following procedures described in the Supporting Information File.

2.9 | Preparation of R18-Labeled N09 and Fluorescence Release Assay

Ethanolic R18 (octadecyl rhodamine B chloride, Sigma Aldrich, 3.12 µmol/mL) was added to a N09 suspension (2 mg/mL of viral protein). The mixture was incubated in the dark for 1 h at RT. Non-incorporated fluorophores were removed using Zeba Spin Desalting columns (7 K MWCO, Thermo Fisher Scientific, Waltham, MA) with 10 mM TES and 150 mM NaCl (pH 7.4) as elution buffer. Two µg/mL of R18-labeled N09 in DMEM medium were incubated with 100 µg/mL of nonfunctionalized CD, 1% Triton X-100, or 100 µg/mL CD-SA and incubated for 3 h. Fluorescence was measured using a Tecan Infinite 200 plate reader (560 nm excitation, 590 nm emission).

2.10 | Antiviral Resistance Assay

H1N1/pdm09 was passaged nine times (0.1 PFU/cell) in Calu-3 cells, seeded in six-multiwell plates, in the presence of

increasing concentrations of CD-SA, CD-6′SLN (from 1 to 256 µg/mL for CD-SA and from 1 to 4 µg/mL for CD-6′SLN), and combined therapy of CD-SA (from 1 to 256 µg/mL) with IFNλ1 (from 15 to 960 ng/mL) or in presence of serum-free MEM. CD-SA and CD-6′SLN were administered 1 hpi, after inoculum removal. IFNλ1 was given to the cells 24 h before infection (hbi) and again 1 hpi. After 48 h, supernatants were collected and centrifuged at 3000 rpm for 5 min to remove dead cells and viral loads were quantified by titration in MDCK cells. Viruses presenting increased viral loads were sequenced and the drug sensitivity was checked via a dose–response assay.

2.11 | RT-qPCR Analysis, Viral RNA Quantification and Sequencing

Viral RNA was extracted and quantified using RT-qPCR as previously described [12]. For sequencing, viral genomes were extracted, reverse-transcribed, purified, and sequenced (Fasteris DNA sequencing service, Geneva). Sequences were analyzed with Geneious software.

2.12 | In Vivo Mouse Model

Female 18−20 g BALB/c mice were obtained from Charles River Laboratories (Wilmington, MA). Detailed procedure of mice experiments is available in the Supporting Information File. All animal procedures complied with USDA guidelines and were conducted at AAALAC-accredited animal research facilities at Utah State University under protocol #12379, approved by the Utah State University Institutional Animal Care and Use Committee.

2.13 | Statistical Analysis

Statistical analysis was performed using GraphPad Prism 7 software. Results are expressed as means ± SD of two independent experiments or 10 animals per group. Results were analyzed by Student's t-test or two-way ANOVA test when more than two groups or multiple time points were analyzed. A value of $p < 0.05$ was considered significant. $*p < 0.05$; $**p < 0.01$; $***p < 0.001$.

3 | Results

3.1 | CD-SA Inhibits Infection of A/Netherlands/602/2009 (H1N1)pdm09 by Direct Binding to HA Protein and via a Virucidal Mechanism

The antiviral effect of CD-SA (Figure 1A) against IV A/Netherlands/602/2009 (H1N1)pdm09 (named hereafter N09) was compared to that of CD-6′SLN (Figure 1B) in virus-pretreatment conditions. Viruses (500 PFU) were pretreated 1 h with the molecule at 37°C before infection of MDCK cells. In these conditions, the EC_{50} of CD-SA was 4.75 ng/mL (Figure 2A), ≈25 to 40 times lower than that of CD-6′SLN (120 ng/mL), and the cytotoxic concentration 50 (CC_{50}) was > 1000 µg/mL, the highest concentration tested in MDCK cells (Table 1). To assess the antiviral mechanism of action, CD-SA was applied in three additional conditions: cell pretreatment, virus cotreatment at the time of infection, or posttreatment 1 h after infection. As shown in Figure 2B, none of these conditions was as effective as the virus pretreatment condition (Figure 2A). The cotreatment was the second most effective (96.55 ± 15% inhibition at 100 µg/mL), while a weak inhibition was observed in both cell pretreatment (30 ± 19.5% inhibition at 100 µg/mL) and posttreatment conditions (19.5 ± 16.9% inhibition at 100 µg/mL). These results indicate that the antiviral effect of CD-SA is based on the compound−virus interaction, rather than a cell-mediated effect.

We next assessed whether CD-SA, like other CD-based antivirals [10, 18], irreversibly disrupts viral integrity (Figure 3). We performed a virucidal assay (Figure 3A and Table 1). Specifically, we incubated 1E6 PFU of N09 with the EC_{90} CD-SA concentration (57 ng/mL) for 3 h at 37°C. After incubation, we assessed the virus's residual infectivity through serial dilutions
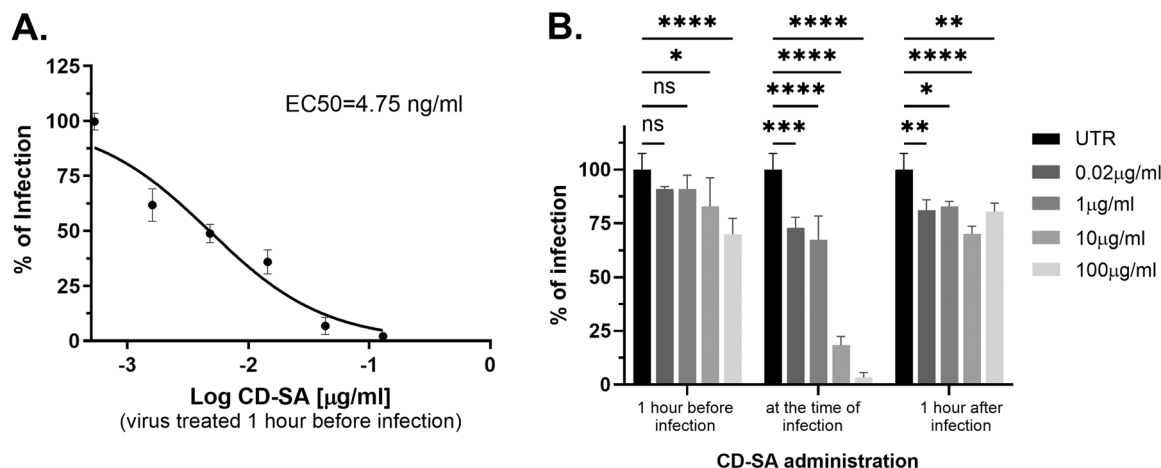
FIGURE 2 | Antiviral action of CD-SA against N09. Dose–response assay of CD-SA against N09 in virus pretreatment condition (A) and efficacy depending on time of administration (B). In (B), MDCK cells were either pretreated with CD-SA for 1 h before infection; cotreated at the time of infection; or treated with CD-SA 1 h after infection. Percentages of infection are shown as mean and SD. p-values ($*\leq 0.1$; $**\leq 0.01$; $***\leq 0.001$; $***\leq 0.0001$) were calculated using two-way ANOVA.

TABLE 1 | Dose–response and virucidal activity of CD-SA in MDCK cells against several IV-A and IV-B strains and against SARS-CoV-2 and HPIV3, two viruses known to use sialic acid to attach to the host cells. Results present the mean of two independent experiments performed in duplicate (95% confidence interval [CI]).

Viral strain	CD-SA and CD-6SLN CC$_{50}$ [µg/mL]	CD-SA EC$_{50}$ [µg/mL] [CI]	SI	Virucidal activity	CD-6SLN EC$_{50}$ [µg/mL] [CI]	SI	Virucidal activity
A/Netherlands/602/2009 (H1N1)pdm09	> 1000	0.0048 [0.0036 to 0.0062]	> 208 333	++	0.12 [0.11 to 0.14]	> 1666	++
A/Switzerland/02824/2022 (H1N1)pdm09	> 1000	7.14 [5.37 to 10.31]	> 140	+	5.96 [4.54 to 8.3]	> 167.8	+
A/Wyoming/03/2003 (H3N2)	> 1000	0.064 [0.052 to 0.08]	> 15 625	++	0.088 [0.073 to 0.1]	> 12 500	++
A/Switzerland/4955/2019 (H3N2)	> 1000	10.54 [6.85 to 15.24]	> 94.87	—	7.54 [5.3 to 10]	> 132.6	—
B/Wisconsin/01/2010 Yamagata-Lineage	> 1000	27.8 [15.92 to 51.79]	> 35.9	++	4.76 [3.1 to 6.4]	> 210.1	++
B/Switzerland/88277/2018 Yamagata-Lineage	> 1000	0.515 [0.189 to 1.067]	> 1941	++	0.72 [0.34 to 1.27]	> 1388.9	++
B/Switzerland/47324/2024 Victoria-Lineage	> 1000	314.8 [212.6 to 516.5]	> 3.18	—	5.9 [3.7 top 9.1]	> 169.5	+
hCoV-19/Switzerland/VD-HUG-36221084/2021 B.A.1 Variant	> 5000[a]	232 [156.6 to 364.9]	> 21.55	—	8.27 [6.78 to 9.8]	> 604.6	—
Para Influenza 3	> 1000[b]	> 500	< 1	NA	> 500	< 1	NA

Note: [a]VeroE6 cells and [b]A549 cells. A virucidal activity leading to a reduction of viral titers of more than one log in the virucidal assay is considered as a strong virucidal activity (++), a reduction of +/− one log is still considered as virucidal (+), and a reduction below one log is considered as non-virucidal (−). The detailed virucidal assay results are available in the Figure S1 [10].
Abbreviations: CC50, cytotoxic concentration 50 calculated in cells; EC50, effective concentration 50 calculated in the same cell lines.
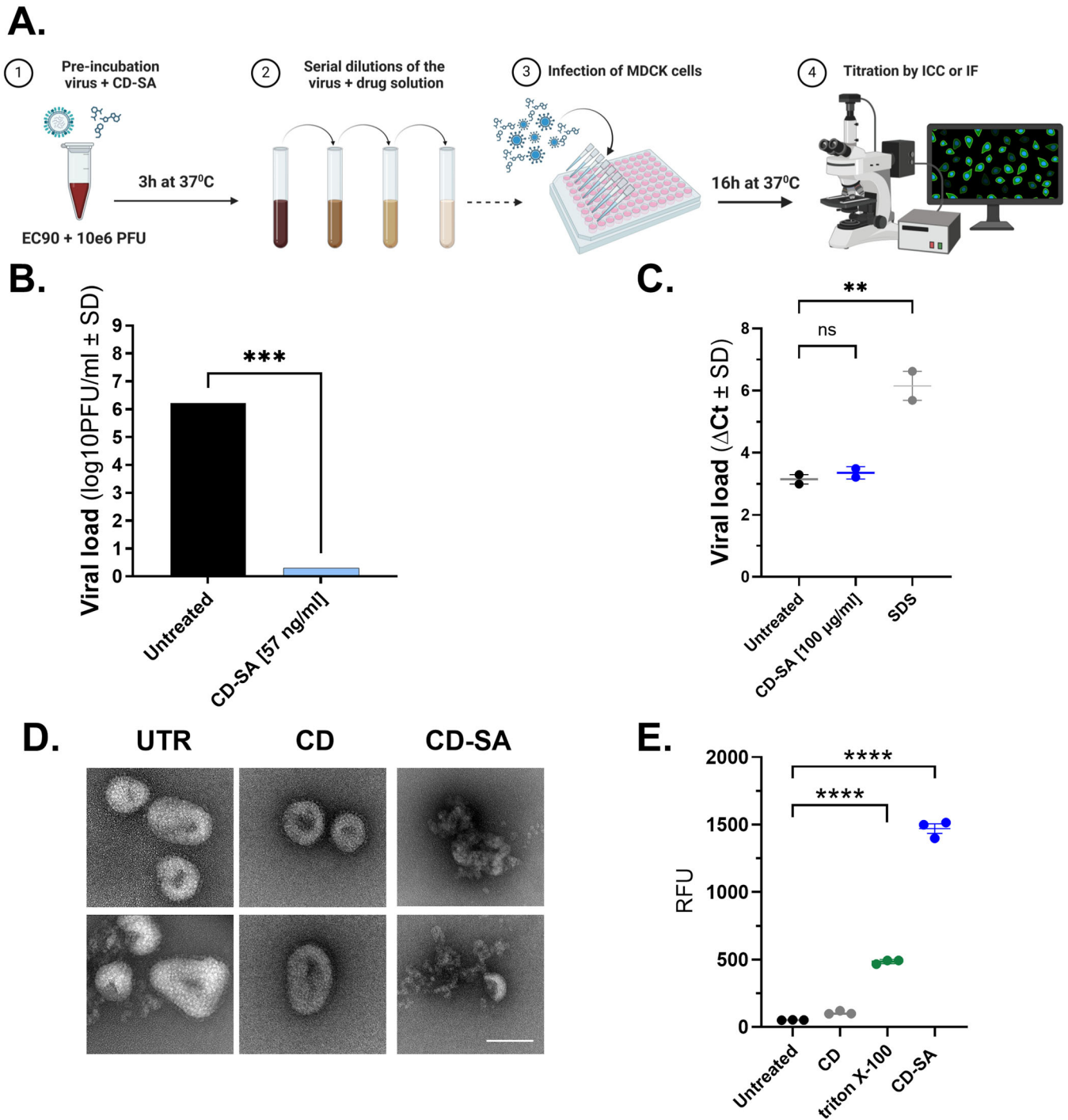
FIGURE 3 | Virucidal activity of CD-SA against N09. (A) Schematic representation of the protocol. (B) Virucidal assay: N09 and CD-SA (EC_{90} = 57 ng/mL) or the CD-SA vehicle (UTR) were incubated for 3 h at 37°C and serially diluted onto MDCK cells and viral titers were evaluated by immunocytochemistry. A reduction of viral titer by > 1 log indicates a virucidal mechanism of action [10]. The ***$p \leq 0.001$ was determined using an unpaired t-test. (C) RNA exposure assay: Cycle threshold difference in N09 RT-qPCR between RNase-treated (SDS) virus molecule mixture (100 µg/mL) and buffer-treated virus molecule mixture (untreated condition = UTR). The **$p \leq 0.01$ was determined using an ordinary one-way ANOVA. (D) Negative staining electron microscopy of N09 incubated with a control medium or 1.7 µg/mL of nonfunctionalized CD, or virucidal CD-SA for 1 h at 37°C. Scale bar: 50 nm. (E) Envelope integrity assay: Relative fluorescence unit of R18-labeled N09 measured after 3 h incubation with nonfunctionalized CD, triton X-100, and CD-SA. ****$p \leq 0.0001$ were determined using one-way ANOVA.

of the virus/drug complex. In cases of virustatic effects, viral infectivity fully recovers upon dilution, while with virucidal effects, infectivity does not recover after dilution, even when the final drug concentration is lower than the drug EC_{50} [10, 18]. To distinguish between these outcomes, we compared the treated virus (incubated with the drug) to the untreated control (virus incubated with the drug dilution buffer alone). After dilutions, samples were used to infect cells, and we determined the virus titer through immunocytochemistry. As shown in Figure 3B, viral infectivity was greatly decreased even at N09/CD-SA

dilutions leading to a final drug concentration lower than the EC_{50}, confirming an irreversible viral inactivation. Surprisingly, the RNA exposure assay performed as previously described [11] showed that incubation with CD-SA (at $100 \mu g/mL$) did not significantly change the ΔC_t between RNAse treated and buffer-treated virus, compared to the untreated virus, while the positive SDS control resulted in an approximately eightfold increase of the ΔC_t (Figure 3C). This indicates that, unlike SDS, CD-SA does not make the RNA accessible to RNase activity. However, this does not mean that the viral envelope is intact, as the viral nucleoprotein provides another layer of protection for the viral RNA. To study the impact of CD-SA on the viral envelope, we imaged its effect on the N09 structure by TEM and observed that the viral envelope is destroyed by CD-SA incubation, confirming its virucidal effect (Figure 3D). These results were also supported by a fluorescent release assay (Figure 3E), in which the envelope of N09 was labeled with the amphiphilic octadecyl rhodamine B chloride (R18) dye before incubation with nonfunctionalized CD, CD-SA, and Triton X-100. In the two latter situations, the relative fluorescence unit (RFU) was significantly increased compared to the untreated virus, while the nonfunctionalized CD showed no difference.

3.2 | CD-SA Displays Direct Antiviral Activity Against Different Influenza Subtypes and Against SARS-CoV-2 Omicron Variant

As CD-SA exposes a unique SA epitope covalently bound to an undecyl linker, it is expected to bind the HA pocket of several IV strains and potentially also the glycoproteins of other SA-dependent viruses. Hence, we compared the spectrum of activity of CD-SA and CD-6′SLN against a wide range of IV A and IV B strains as well as two other SA-dependent viruses, HPIV3 and SARS-CoV-2 Omicron B.A.1 (Table 1 and Figure S1). We pre-incubated viruses with serial drug dilutions before infection to determine the drug EC50 (Table 1, Columns 3 and 6) and we also assessed the virucidal activity (Table 1, Columns 5 and 8).

The EC50 and virucidal activity of both compounds were comparable against the different H1N1 strains tested, although the EC50 of CD-SA was significantly lower against N09 (0.0048 vs. $0.12 \mu g/mL$). The activity against recent H1N1 strains (A/Switzerland/02824/2022) was significantly less potent (7.14 and $5.96 \mu g/mL$ for CD-SA and CD-6′SLN, respectively) but remained virucidal. The two compounds turned out to be also very active and virucidal against A/Wyoming/03/2003 (H3N2) (EC50 of 0.064 and $0.088 \mu g/mL$ for CD-SA and CD-6′SLN) and against A/Singapore/37/2004 (H3N2) ([10] and data not shown), but the activity was reduced against A/Switzerland/4955/2019 (H3N2) (EC50 of 10.54 and $7.54 \mu g/mL$ for CD-SA and CD-6′SLN) and the virucidal effect was lost for both compounds. Concerning influenza B (IV B) strains from the Yamagata lineage, the two compounds demonstrated both antiviral and virucidal activity. Notably, the EC50 values improved significantly against the most recent strain, B/Switzerland/88277/2018 (Yamagata lineage), compared to the older strain, B/Wisconsin/01/2010 (Yamagata lineage). Specifically, EC50 values were $0.515 \mu g/mL$ for CD-SA and $0.72 \mu g/mL$ for

CD-6′SLN against the recent strain, in contrast to $27.8 \mu g/mL$ for CD-SA and $4.76 \mu g/mL$ for CD-6′SLN against the older strain.

Altogether both CD-SA and CD-6′SLN present selectivity index > 35 against circulating IV A strains and against IV B Yamagata, confirming their broad-spectrum anti-IV activity. However, although both molecules retained activity against B/Switzerland/47324/2024 Victoria-Lineage, the selectivity index turned out to be below 10 for CD-SA while it was still high for CD-6′SLN. Moreover, CD-6′SLN showed a virucidal activity in contrast of CD-SA. We finally assessed CD-SA and CD-6′SLN efficacy against SARS-CoV-2 hCoV-19/Switzerland/VD-HUG-36221084/2021 B.A.1 variant and against HPIV3, two viruses known to use SA moieties as a binding anchor. Albeit no effect was observed against HPIV3, both compounds were active and virustatic against the SARS-CoV-2 Omicron B.A.1 variant with lower EC50 for CD-6′SLN (EC50 of 232 vs. $8.27 \mu g/mL$, respectively) (Table 1). These data indicate that the activity of both CD-SA and CD-6′SLN is broad and can extend to other SA-dependent viruses and that the efficacy and virucidal effect depend on the SA linkage type.

3.3 | CD-SA Displays Antiviral Activity in Respiratory Tissue Culture Model

We previously showed that CD-6′SLN blocks IV infections in ex vivo reconstituted human respiratory tissues [13]. Here, we conducted a similar test for CD-SA, with CD-6′SLN serving as control. We infected reconstituted HAE with 1E5 RNA copies of N09 and treated them daily for 5 days, starting at 1 dpi. We then daily monitored the amount of virus released from the apical tissue side (Figure 4A). We observed a significant reduction of viral replication in treated versus untreated tissues, confirming the therapeutic potential of CD-SA in this relevant tissue culture model (Figure 4B). Of note, no change in metabolic activity was observed in treated versus untreated tissues at this compound concentration (Figure 4B, dashed line).

3.4 | CD-SA Genetic Barrier to Resistance In Vitro

We next compared the genetic barrier to resistance to CD-SA or CD-6′SLN during nine serial passages of N09 in Calu-3 cells (Table 2 and Figure S2). Calu-3 were used as they express proteases which allows multiple cycles of infection without addition of trypsin [19]. One $\mu g/mL$ (a dose that enables good viral replication despite antiviral pressure) of compound was administered 1 hpi and the drug concentration was doubled at each passage (up to $256 \mu g/mL$). An untreated control was added to monitor cell adaptation which could spontaneously occur during the passages. At 48 hpi, the infectious viral titers were measured by plaque assay in MDCK cells.

An increase in viral titer was already observed at passage 2 (P2) under CD-6′SLN treatment (Figure S2A). In contrast, a comparable and significant loss of effectiveness was observed only at
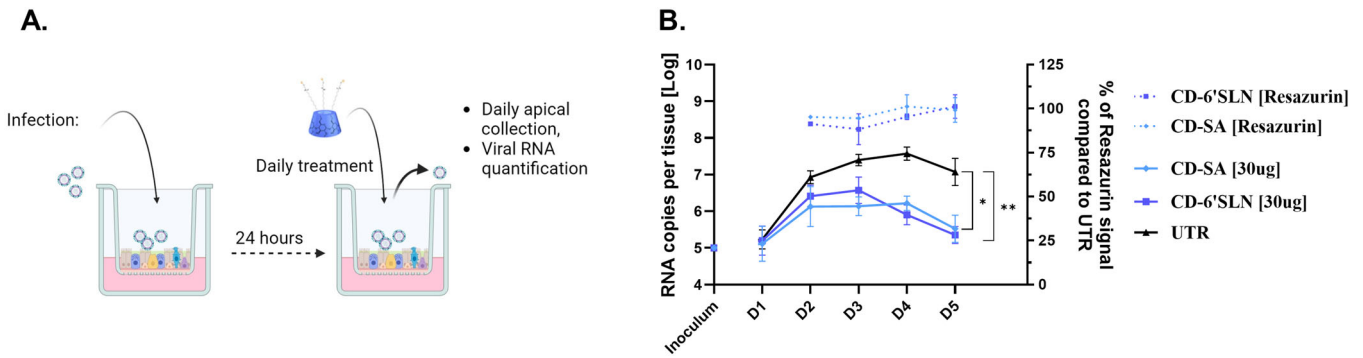
A.

B.

FIGURE 4 | Antiviral efficacy of CD-SA and CD-6′SLN against N09 in ex vivo human airway epithelia (HAE) reconstituted at the air-liquid interface. (A) Schematic of ex vivo HAE infection and treatment. (B) Tissues were infected apically and antivirals were administered from 1 to 4 dpi. Cell viability of uninfected treated controls was assessed by resazurin assay (dashed lines). Viral loads were daily quantified by RT-qPCR. The results represent the mean and SD from two independent experiments. Statistics were obtained by analyzing the AUC (area under the curve). $*p \leq 0.1$; $**p \leq 0.01$.

TABLE 2 | Emergence of resistance of N09 after passages in presence of increasing concentrations of CD-6′SLN, CD-SA, or a combined CD-SA/IFNλ1 treatment.

Drug selection	Passage[a]	HA mutation[b]	CD-6′SLN EC$_{50}$ [µg/mL][c]	CD-SA EC$_{50}$ [µg/mL][c]
Untreated	4	D127E	2.7	2.61
CD-6′SLN	2	Q223Q/R	—	—
	3	Q223R	> 100	—
CD-SA	4	D127E	—	13.47
	6	K211N/R221K	—	128.3
	8	K211N/R221K	—	214.5
IFNλ1 + CD-SA	4	D127E	—	3.4
	8	K154E	—	3.96

[a]Passage number where mutations were detected.
[b]Mutations numbered according to H1 pdm09 numbering [20].
[c]Results obtained from duplicate experiments.

P5 for CD-SA (Figure S2B), indicating that CD-SA presents a higher genetic barrier to antiviral resistance. Finally, cotreatment with IFNλ1 prevented the emergence of resistance against CD-SA over all nine passages, as it has been previously shown for oseltamivir (OS) [21].

We sequenced the HA gene and performed the EC50 of viruses collected at different passages (Table 2 and Figure S2). We identified a mutation present in the HA of all variants from passage 4 (D127E), including the untreated control, which is very likely due to an adaptation to Calu-3 cells (Table 2). Resistance to CD-6′SLN was associated with the HA Q223R mutation which became dominant at P3, already identified in our previous study [21] and known to change receptor preference from human α2-6 to avian α2-3 linked SA [22]. Of note, N09 is mice-adapted and, therefore, has a higher affinity for α2-3 bound SA that predominates in the mouse respiratory tract. A significant increase in the EC$_{50}$ of CD-SA was associated with the K211N/R221K mutations detected at P6. The role of these two mutations is less well-established. R221K, along with five other mutations, has been shown to increase the virulence of pandemic H1N1 in mice, a phenotype associated with enhanced binding to α2-3 linked SA and decreased binding to α2-6 linked SA [23]. Finally, the K154E mutation identified at

P6 in the combined treatment did not cause a significant shift in the EC$_{50}$ and probably emerged randomly.

3.5 | Antiviral Activity of CD-SA in Mice

We then investigated CD-SA effect in vivo. Toxicity experiments were performed with 5−80 mg/kg of CD-SA administered intranasally (i.n.) and for 6 days. Up to 10% weight loss was observed between Days 5 and 7 with the 60 and 80 mg doses, but mice weight returned to normal afterwards (Figure S3). For efficacy assay, female BALB/c mice (10 per group) were infected i.n. with 30 CCID$_{50}$ of A/California/04/2009 and then treated once daily i.n. and for 5 days with 7.5 or 40 mg/kg of CD-SA starting from 1 or 2 dpi (Figure 5). A group of mice treated per OS twice daily for 5 days with 30 mg/kg/day of OS (starting 2 h before infection) was added as a positive control. Contrary to OS treatment that only delayed mouse death by 2 days (no survival observed), CD-SA significantly increased survival rate when administered from both 1 dpi (7.5 mg/kg, 40% of survival; 40 mg/kg, 60% of survival; $p < 0.001$) or 2 dpi (7.5 mg/kg, 70% of survival; 40 mg/kg, 70% of survival; $p < 0.001$). Interestingly, the survival rate was higher for mice treated after 2 days and the

A. Treatment 1 day post infection
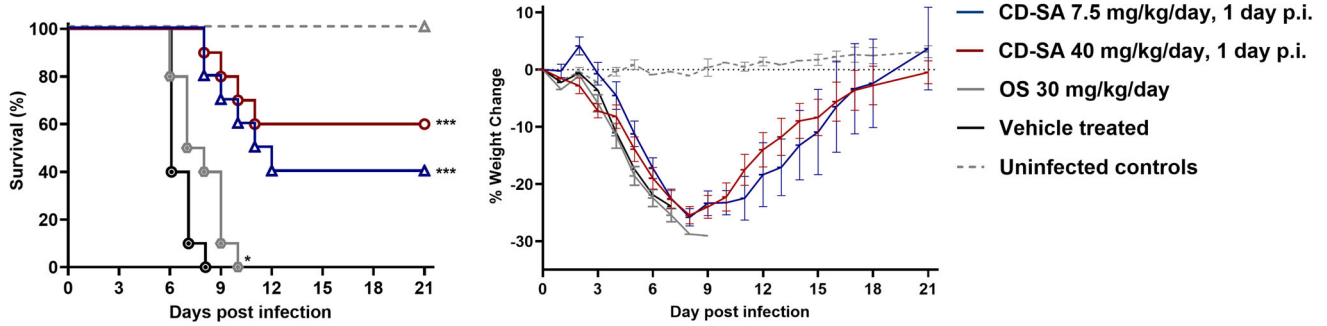
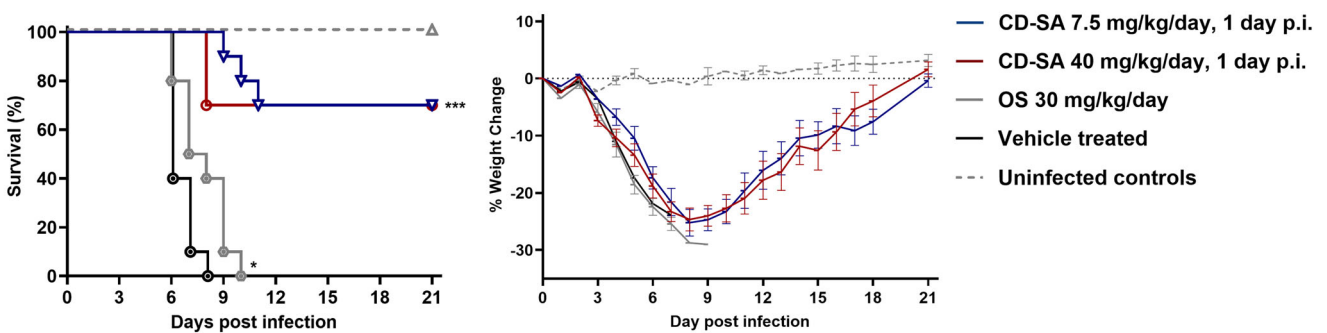## B. Treatment 2 days post infection

FIGURE 5 | Efficacy of CD-SA and oseltamivir (OS) against influenza A/California/04/2009 in BALB/c mice. Female mice (10/group) were infected and intranasally treated with sterile saline (vehicle) or CD-SA after 1 (A) or 2 dpi (B) and continued for 5 days. Control mice were treated by oral gavage with OS, 2 h before infection and twice daily afterwards for 5 days. Survival curves (left panels) and percentages of weight changes (right panels) are shown. Survival rates were compared by the Mantel−Cox log-rank test using Prism 9 (GraphPad Software, San Diego, CA). ***$p < 0.001$, *$p < 0.05$ compared to the vehicle-treated animals. The mean weight of surviving mice at the different days postinfection was computed and plotted.

same survival rate was observed for mice treated with 7.5 or 40 mg/kg of CD-SA.

4 | Discussion

Influenza presents an important pandemic risk and IV epidemics cause severe disease and death worldwide. The Centers for Disease Control (CDC) estimates that each year, influenza is responsible for 100 000−710 000 hospitalizations and 5−50 000 deaths in the United States of America [24]. Therapies are still wanting, with seasonal vaccines at the forefront and limited antiviral treatment alternatives. To tackle these challenges, novel anti-IV antivirals targeting HA, the most abundant IV surface protein, have been proposed. HA forms a weak bond with oligosaccharides terminating with SA (N-acetylneuraminic acid, Neu5Ac) [25], which prompted researchers to opt for multivalent macromolecular strategies. This has led to several macromolecules that present SA such as polymer scaffolds [26, 27], DNA-based macromolecules [28], virus-like particles [29], micelles and lipid bilayers [30–32], gold nanoparticles [33] and protein scaffolds [34–36], among other sialylated macromolecular decoys for IVs. Unfortunately, in vivo efficacy has not been demonstrated or addressed for most of these molecules. One possible explanation is that these glycoclusters represent a virustatic decoy for IV that does not destroy the infective particle. Hence, as the concentration of the drug decreases, infective viruses are free to infect host cells. Unlike all these approaches, CD-SA is based on a molecular architecture that

exerts a hydrophobic force on the virus, leading to irreversible damage, rendering it noninfective [10, 18, 37]. This property sets CD-SA aside from most other glycoclusters and sialylated molecules.

Here, we show a strong antiviral efficacy against H1N1 pandemic strains in vitro, ex vivo, and in vivo. Our in vivo results demonstrate the efficacy of CD-SA in rescuing mice from a lethal IV infection when added 24 or 48 h postinfection, while OS proves ineffective even if given before infection and twice daily afterwards (Figure 5). The therapeutic window of CD-SA is thus longer than that of a shedding inhibitor, likely due to the virucidal action directly on infective viral particles. The in vivo results also show that the dose range and time of administration of CD-SA can be optimized as the lowest dose of 7.5 mg/kg/day, when administered at 2 dpi, rescued as many animals as the dose of 40 mg/kg/day.

The in vivo results can be explained by the fact that CD-SA destroys the viral envelope likely after interaction with the HA, as demonstrated by the electron micrographs (Figure 3C) and fluorescence release assay (Figure 3D) of IVs exposed to CD-SA. Interestingly, the RNA release assay did not yield a significant RNA degradation after exposure to CD-SA, this is likely because the molecule does not break the interaction between the nucleoprotein and the RNA. Upon examining all electron micrographs of IVs in the presence of CD-SA, it is evident that the viral particles are thoroughly distorted, indicating a probable release of their contents due to the mechanism of action of

CD-SA. This mechanism explains the virucidal effect shown in Figure 2 and, ultimately, the survival curves of mice treated with this molecule. This may also explain why the molecules appear more active when administered 2 days postinfection compared to 1 day. Optimal virucidal effects are achieved when a significant number of extracellular virions come into contact with the molecules. Therefore, the in vivo kinetics of the infection and the time required for the compounds to reach the primary site of viral replication may influence the efficacy of the administered virucidal compounds.

We then compared the antiviral activity of CD-SA with CD-6'SLN, a molecule functionalized with 6'SLN to closely resemble the receptor of human IV strains. Since the molecule CD-SA is functionalized with a single SA residue, we initially anticipated broader antiviral activity. However, both compounds ultimately demonstrated efficacy against IV A H1N1, H3N2, and IV B strains from both the Yamagata and Victoria lineages. However, despite this shared broad-spectrum activity, their efficacy varied significantly: CD-SA was more potent against H1N1 N09, while CD-6'SLN was more effective against the IV B Victoria strain. Furthermore, while both molecules lost virucidal effect against recent H3N2 variants, CD-6'SLN but not CD-SA retained virucidal activity against the IV B Victoria strain from 2024. Although IV B, IV A H1N1, and H3N2, all use α2-6 bound SA as a receptor, the branching in recent H3N2 and IV B Victoria strains may be more complex and variable, or the envelope structure may offer greater resistance to external pressures [38]. Notably, both compounds also showed virustatic antiviral activity against the SARS-CoV-2 Omicron variant. Overall, these findings highlight the potential of SA-mimicking compounds to broadly target IVs and potentially other SA-dependent viruses but also emphasize the need for further development to achieve broader virucidal activity across all human-infecting IV strains and other virus groups.

OS and Baloxavir Marboxil are FDA-approved drugs used to treat IV-infected patients. However, mutations conferring resistance to these compounds have been documented [39–41]. Here, we observed that the emergence of resistance mutations against CD-SA emerged after six passages in Calu-3 cells, while the resistance to CD-6'SLN emerged already after three passages, indicating that the barrier to resistance is higher for CD-SA than for CD-6'SLN (Table 2). We also identified that mutations conferring resistance against CD-SA (K211N/R221K) differed from those found in the presence of CD-6'SLN (Q223R), the latter being known to cause a switch in receptor usage from α2-6 bound SA to α2-3 bound SA [42]. HA normally binds to longer oligosaccharides that terminate with SAs, with high specificity to the sequence and connectivity between the sugar monomers. For example, avian strains of IV bind to α2-3 SA on lactosamine and mammalian strains to α2-6 linkages. In using a SA directly connected to an aliphatic chain, the evolutionary pressure to adapt to the compound was no longer naturally occurring as a connectivity adaptation, but rather to a SA presented directly to the binding pocket. This can explain the higher barrier to resistance observed for CD-SA when compared to CD-6'SLN as well as the different resistant mutations identified. This higher barrier to resistance urges for further investigation of this macromolecule as a promising antiviral agent that targets HA. In addition, as shown previously for OS [20],

combining CD-SA with IFNλ1 prevented emergence of antiviral resistance over nine serial passages (Table 2). Combination therapies coupling virucidal compounds and endogenous antiviral molecules with low inflammatory profiles, may thus represent promising approaches to limit emergence of IV-resistant variants.

In conclusion, CD-SA shows enormous potential as a novel anti-IV antiviral. Its virucidal mechanism of action correlates with in vivo efficacy, and further optimization of this compound and development toward the use against influenza can introduce a valuable addition to the toolkit to manage morbidity and prevent the mortality caused by influenza infection, thus enhancing the preparedness for a pandemic.

Author Contributions

Arnaud Charles-Antoine Zwygart: conceptualization, methodology, investigation, writing–original draft, writing–review and editing, visualization. **Chiara Medaglia:** conceptualization, methodology, investigation, writing–original draft, writing–review and editing. **Yong Zhu:** methodology, investigation, writing–original draft, review and editing, visualization. **E. Bart Tarbet:** investigation, review and editing. **Westover Jonna:** investigation, review and editing. **Clément Fage:** review and editing. **Didier Le Roy:** investigation. **Thierry Roger:** resources, review and editing. **Sophie Clément:** writing–review and editing. **Samuel Constant:** resources, review and editing. **Song Huang:** methodology, resources, review and editing. **Francesco Stellacci:** conceptualization, resources, review and editing. **Paulo Jacob Silva:** conceptualization, writing–original draft, writing–review and editing, visualization. **Caroline Tapparel:** conceptualization, resources, writing–review and editing, visualization, supervision, project administration, funding acquisition.

Acknowledgments

Ethics Statement

The animal study was conducted in accordance with the approval of the Institutional Animal Care and Use Committee of Utah State University and done in the AAALAC-accredited Laboratory Animal Research Center of Utah State University.

Conflicts of Interest

The authors declare no conflicts of interest.

Data Availability Statement

Data will be made available on request.

References

1. S. Knobler, A. Mahmoud, S. Lemon, and L. Pray, eds., *The Impact of Globalization on Infectious Disease Emergence and Control: Exploring the Consequences and Opportunities: Workshop Summary* (Washington DC: National Academies Press, 2006).

2. J. S. Long, B. Mistry, S. M. Haslam, and W. S. Barclay, "Host and Viral Determinants of Influenza A Virus Species Specificity," *Nature Reviews Microbiology* 17, no. 2 (2019): 67–81.

3. P. Saunders-Hastings and D. Krewski, "Reviewing the History of Pandemic Influenza: Understanding Patterns of Emergence and Transmission," *Pathogens* 5, no. 4 (2016): 66.

4. L. P. Tavares, M. M. Teixeira, and C. C. Garcia, "The Inflammatory Response Triggered by Influenza Virus: A Two Edged Sword," *Inflammation Research* 66, no. 4 (2017): 283–302.

5. M. Essaidi-Laziosi, F. Brito, S. Benaoudia, et al., "Propagation of Respiratory Viruses in Human Airway Epithelia Reveals Persistent Virus-Specific Signatures," *Journal of Allergy and Clinical Immunology* 141, no. 6 (2018): 2074–2084.

6. D. M. Morens, J. K. Taubenberger, and A. S. Fauci, "Predominant Role of Bacterial Pneumonia as a Cause of Death in Pandemic Influenza: Implications for Pandemic Influenza Preparedness," *Journal of Infectious Diseases* 198, no. 7 (2008): 962–970.

7. N. M. Bouvier and P. Palese, "The Biology of Influenza Viruses," supplement, *Vaccine* 26, no. S4 (2008): D49–D53.

8. R. J. Connor, Y. Kawaoka, R. G. Webster, and J. C. Paulson, "Receptor Specificity in Human, Avian, and Equine H2 and H3 Influenza Virus Isolates," *Virology* 205, no. 1 (1994): 17–23.

9. K. Shinya, M. Ebina, S. Yamada, M. Ono, N. Kasai, and Y. Kawaoka, "Influenza Virus Receptors in the Human Airway," *Nature* 440, no. 7083 (2006): 435–436.

10. O. Kocabiyik, V. Cagno, P. J. Silva, et al., "Non-Toxic Virucidal Macromolecules Show High Efficacy Against Influenza Virus Ex Vivo and In Vivo," *Advanced Science* 8, no. 3 (2021): 2001012.

11. Y. Zhu, A. A. Sysoev, P. H. J. Silva, M. Batista, and F. Stellacci, "Antiviral Mechanism of Virucidal Sialic Acid Modified Cyclodextrin," *Pharmaceutics* 15, no. 2 (2023): 582.

12. C. Medaglia, I. Kolpakov, A. C. A. Zwygart, et al., "An Anti-Influenza Combined Therapy Assessed by Single Cell RNA-Sequencing," *Communications Biology* 5, no. 1 (2022): 1075.

13. R. Heida, Y. C. Bhide, M. Gasbarri, et al., "Advances in the Development of Entry Inhibitors for Sialic-Acid-Targeting Viruses," in *Drug Discovery Today*. Vol. 26 (Groningen: Elsevier Current Trends, 2021), 122–137.

14. L. Nguyen, K. A. McCord, D. T. Bui, et al., "Sialic Acid-Containing Glycolipids Mediate Binding and Viral Entry of SARS-CoV-2," *Nature Chemical Biology* 18, no. 1 (2022): 81–90.

15. A. Scheid, L. A. Caliguiri, R. W. Compans, and P. W. Choppin, "Isolation of Paramyxovirus Glycoproteins. Association of Both Hemagglutinating and Neuraminidase Activities With the Larger SV5 Glycoprotein," *Virology* 50, no. 3 (1972): 640–652.

16. H. Tozawa, M. Watanabe, and N. Ishida, "Structural Components of Sendai Virus," *Virology* 55, no. 1 (1973): 242–253.

17. A. C. Zwygart, C. Medaglia, R. Huber, et al., "Antiviral Properties of Trans-Delta-Viniferin Derivatives Against Enveloped Viruses," *Biomedicine and Pharmacotherapy* 163 (2023): 114825.

18. S. T. Jones, V. Cagno, M. Janeček, et al., "Modified Cyclodextrins as Broad-Spectrum Antivirals," *Science Advances* 6, no. 5 (2020): eaax9318.

19. E. Böttcher-Friebertshäuser, D. A. Stein, H. D. Klenk, and W. Garten, "Inhibition of Influenza Virus Infection in Human Airway Cell Cultures by an Antisense Peptide-Conjugated Morpholino Oligomer Targeting the Hemagglutinin-Activating Protease TMPRSS2," *Journal of Virology* 85, no. 4 (2011): 1554–1562.

20. D. F. Burke and D. J. Smith, "A Recommended Numbering Scheme for Influenza A HA Subtypes," *PLoS One* 9, no. 11 (2024): e112302.

21. C. Medaglia, A. C. A. Zwygart, P. J. Silva, et al., "Interferon Lambda Delays the Emergence of Influenza Virus Resistance to Oseltamivir," *Microorganisms* 9, no. 6 (2021): 1196.

22. O. Suptawiwat, W. Jeamtua, Ch Boonarkart, A. Kongchanagul, P. Puthawathana, and P. Auewarakul, "Effects of the Q223R Mutation in the Hemagglutinin (HA) of Egg-Adapted Pandemic 2009 (H1N1) Influenza A Virus on Virus Growth and Binding of HA to Human- and Avian-Type Cell Receptors," *Acta Virologica* 57, no. 3 (2013): 333–338.

23. N. A. Ilyushina, A. M. Khalenkov, J. P. Seiler, et al., "Adaptation of Pandemic H1N1 Influenza Viruses in Mice," *Journal of Virology* 84, no. 17 (2010): 8607–8616.

24. CDC, "Disease Burden of Flu." (2024), https://www.cdc.gov/flu.

25. N. K. Sauter, M. D. Bednarski, B. A. Wurzburg, et al., "Hemagglutinins From Two Influenza Virus Variants Bind to Sialic Acid Derivatives With Millimolar Dissociation Constants: A 500-MHz Proton Nuclear Magnetic Resonance Study," *Biochemistry* 28, no. 21 (1989): 8388–8396.

26. G. B. Sigal, M. Mammen, G. Dahmann, and G. M. Whitesides, "Polyacrylamides Bearing Pendant α-Sialoside Groups Strongly Inhibit Agglutination of Erythrocytes by Influenza Virus: The Strong Inhibition Reflects Enhanced Binding Through Cooperative Polyvalent Interactions," *Journal of the American Chemical Society* 118, no. 16 (1996): 3789–3800.

27. W. J. Lees, A. Spaltenstein, J. E. Kingery-Wood, and G. M. Whitesides, "Polyacrylamides Bearing Pendant Alpha-Sialoside Groups Strongly Inhibit Agglutination of Erythrocytes by Influenza A Virus: Multivalency and Steric Stabilization of Particulate Biological Systems," *Journal of Medicinal Chemistry* 37, no. 20 (1994): 3419–3433.

28. M. Yamabe, K. Kaihatsu, and Y. Ebara, "Sialyllactose-Modified Three-Way Junction DNA as Binding Inhibitor of Influenza Virus Hemagglutinin," *Bioconjugate Chemistry* 29, no. 5 (2018): 1490–1494.

29. C. Nie, B. Parshad, S. Bhatia, et al., "Topology-Matching Design of an Influenza-Neutralizing Spiky Nanoparticle-Based Inhibitor With a Dual Mode of Action," *Angewandte Chemie* 132, no. 36 (2020): 15662–15666.

30. C. T. Guo, C. H. Wong, T. Kajimoto, et al., "Synthetic Sialylphosphatidylethanolamine Derivatives Bind to Human Influenza A Viruses and Inhibit Viral Infection," *Glycoconjugate Journal* 15, no. 11 (1998): 1099–1108.

31. L. Adam, E. Müller, K. Ludwig, et al., "Design and Functional Analysis of Heterobifunctional Multivalent Phage Capsid Inhibitors Blocking the Entry of Influenza Virus," *Bioconjugate Chemistry* 33, no. 7 (2022): 1269–1278.

32. D. Di Iorio, M. L. Verheijden, E. van der Vries, P. Jonkheijm, and J. Huskens, "Weak Multivalent Binding of Influenza Hemagglutinin Nanoparticles at a Sialoglycan-Functionalized Supported Lipid Bilayer," *ACS Nano* 13, no. 3 (2019): 3413–3423.

33. I. Papp, C. Sieben, K. Ludwig, et al., "Inhibition of Influenza Virus Infection by Multivalent Sialic-Acid-Functionalized Gold Nanoparticles," *Small* 6, no. 24 (2010): 2900–2906.

34. X. Meng, M. Yang, Y. Li, et al., "Multivalent Neuraminidase Hydrolysis Resistant Triazole-Sialoside Protein Conjugates as Influenza-Adsorbents," *Chinese Chemical Letters* 29, no. 1 (2018): 76–80.

35. L. M. Artner, L. Merkel, N. Bohlke, et al., "Site-Selective Modification of Proteins for the Synthesis of Structurally Defined Multivalent Scaffolds," *Chemical Communications* 48, no. 4 (2012): 522–524.

36. M. Mühlberg, M. G. Hoesl, C. Kuehne, J. Dernedde, N. Budisa, and C. P. R. Hackenberger, "Orthogonal Dual-Modification of Proteins for the Engineering of Multivalent Protein Scaffolds," *Beilstein Journal of Organic Chemistry* 11 (2015): 784–791.

37. V. Cagno, M. Gasbarri, C. Medaglia, et al., "Sulfonated Nanomaterials With Broad-Spectrum Antiviral Activity Extending Beyond Heparan Sulfate-Dependent Viruses," *Antimicrobial Agents and Chemotherapy* 64, no. 12 (2020): e02001-20.

38. W. Peng, R. P. de Vries, O. C. Grant, et al., "Recent H3N2 Viruses Have Evolved Specificity for Extended, Branched Human-Type Receptors, Conferring Potential for Increased Avidity," *Cell Host & Microbe* 21, no. 1 (2017): 23–34.

39. Y. Abed, A. Saim-Mamoun, and G. Boivin, "Fitness of Influenza A and B Viruses With Reduced Susceptibility to Baloxavir: A Mini-Review," *Reviews in Medical Virology* 31, no. 3 (2021): e2175.

40. D. B. Mendel and R. W. Sidwell, "Influenza Virus Resistance to Neuraminidase Inhibitors," *Drug Resistance Updates* 1, no. 3 (1998): 184–189.

41. E. A. Govorkova, E. Takashita, R. S. Daniels, et al., "Global Update on the Susceptibilities of Human Influenza Viruses to Neuraminidase Inhibitors and the Cap-Dependent Endonuclease Inhibitor Baloxavir, 2018-2020," *Antiviral Research* 200 (2022): 105281.

42. C. A. Meseko, A. Heidari, G. N. Odaibo, and D. O. Olaleye, "Complete Genome Sequencing of H1N1pdm09 Swine Influenza Isolates From Nigeria Reveals Likely Reverse Zoonotic Transmission at the Human-Animal Interface in Intensive Piggery," *Infection Ecology & Epidemiology* 9, no. 1 (2019): 1696632.

Supporting Information

Additional supporting information can be found online in the Supporting Information section.